Journal Name

ARTICLE

Development of a Label-free Raman Imaging Technique for Differentiation of Malaria Parasite Infected from Non-Infected Tissue

Received 00th January 20xx,
Accepted 00th January 20xx

DOI: 10.1039/x0xx00000x

www.rsc.org/

Laura Frame,[a] James Brewer,[b] Rebecca Lee,[b] Karen Faulds,[a] and Duncan Graham*[a]

During malarial infection, the host uses the spleen to clear the malaria parasites, however, the parasites have evolved the ability to bind to endothelial receptors in blood vessels of tissues to avoid removal, known as sequestration, and this is largely responsible for the symptoms and severity of infection. So a technique which could non-invasively diagnose tissue burden could be utilised as an aid for localised malaria diagnosis within tissue. Raman spectroscopy is a label-free imaging technique and can provide unique and chemically specific Raman 'fingerprint' spectrum of biological samples such as tissue. Within this study, Raman imaging was used to observe the changes to the molecular composition of mice spleen tissue under malarial infection, compared with non-infected samples. From analysis of the Raman imaging data, both tissue types showed very similar spectral profiles, which highlighted that their biochemical compositions were closely linked. Principal component analysis showed very clear separation of the two sample groups, with an associated increase in concentration of heme-based Raman vibrations within the infected dataset. This was indicative of the presence of hemozoin, the malaria pigment, being detected within the infected spleen. Separation also showed that as the hemozoin content within the tissue increased, there was a corresponding change to hemoglobin and some lipid/nucleic acid vibrations. These results demonstrate that Raman spectroscopy can be used to easily discriminate the subtle changes in tissue burden upon malarial infection.

Introduction

Malaria is a mosquito-borne infectious disease, caused by the *Plasmodium* parasite[1] and is a leading cause of morbidity and mortality in the developing world.[2] Five species are known to cause malaria infection in humans, with *Plasmodium falciparum* (*P.falciparum*) being responsible for a large number of cases in Africa.[1,3]

During the erythrocytic infection phase, the parasite catabolises up to 80 %[4] of the hosts' hemoglobin. This occurs within the digestive vacuole of the parasite[5] and produces free heme as a by-product (ferrous [Fe^{II}] protoporphyrin IX)[6], which is toxic to the parasite.[5] To detoxify this, the parasite oxidises it to an insoluble, crystalline material known as hemozoin or the malaria pigment.[5,7] At the end of the erythrocytic cycle, red blood cells (RBCs) rupture, releasing hemozoin and parasites into the bloodstream, with the parasites going on to infect further RBCs and continue the cycle of infection. While hemozoin, under physiological conditions, is not degraded and circulates in the bloodstream until it is digested by macrophages present within specific organs.[7] The spleen is the primary organ involved in the development of an immune response[8] during the erythrocytic stage of infection along with the elimination of parasitised RBCs and hemozoin.[9,10] However, *P.falciparum* proteins on the surface of infected erythrocytes give these cells the ability to bind to endothelial receptors in blood vessels of tissue, leading to sequestration[2,11] of these infected cells and hence reduced clearance from the bloodstream.[2] Sequestration of parasites into tissue is largely responsible for the severity and symptoms of infection[12,13], therefore, a technique which could non-invasively detect tissue burden would be a great step forward.

Raman spectroscopy has been extensively used for the identification of malaria infection most commonly *via* the detection of hemozoin. It has been widely reported by groups including Frosch *et al*.[4] and Wood *et al*.[14] that the choice of Raman excitation wavelength is key to gaining selective enhancement of hemoglobin and hemozoin bands over other non-resonant cellular components. Wood *et al*.[15] reported that by exploiting the resonance Raman characteristics of hemozoin, coupled with partial dark field microscopy, there was potential to detect low-pigmented phases of the malaria parasite's life-cycle within infected erythrocytes. More recently, Hobro *et al*.[16] applied resonance Raman imaging to study the progression of malaria infection *via* blood and plasma samples. They showed that within infected blood samples, changes associated with a loss of hemoglobin and an increase in hemozoin could be

[a] Centre of Molecular Nanometrology, Department of Pure and Applied Chemistry, University of Strathclyde, Technology and Innovation Centre, 99 George Street, G1 1RD
[b] Institute for Infection, Immunity and Inflammation, University of Glasgow, G12 8QQ
* Duncan.graham@strath.ac.uk

Electronic Supplementary Information (ESI) available: [details of any supplementary information available should be included here]. See DOI: 10.1039/x0xx00000x

detected after four days of infection. However, hemozoin detection limits were shown to be reduced to only one day, following *Plasmodium* infection, when plasma samples were analysed due to a reduced heme background. Resonance Raman spectroscopy has also been used within a multimodal imaging approach to study the disease mechanisms of murine cerebral malaria.[17] This work by Hackett *et. al*.[17] showed strong evidence that during cerebral malaria infection iron-mediated protein oxidation occurs within the tissue.

These studies highlight how valuable Raman spectroscopic techniques are for the study of biological matrices within malarial infection. Because Raman spectroscopy is a powerful, label-free technique, it can provide a unique and chemically specific Raman 'fingerprint' spectrum of biological samples.[18–20] It has a number of advantages for studying these types of materials including requiring minimal to no sample preparation[18]; being a non-destructive technique[21]; and allowing specific chemical information to be gained without the use of stains.[22] During the pathogenesis of disease, biological alterations occur, which lead to changes in the biochemical composition of affected tissues. These changes in structure, concentration and composition of biomolecules can be reflected in the Raman spectra of tissue samples. Indeed, Raman spectroscopy has been used to study the subtle molecular changes in tissue samples associated with other diseases including, lung[23] cancer; breast[20,24] cancer; and diabetes.[18]

In this work, we used Raman spectroscopic imaging to study the changes in the biochemical composition of mouse spleen tissue sections following infection with the rodent parasite, *Plasmodium berghei* (*P. berghei*). We compared the Raman spectra of infected with non-infected samples to detect changes in the Raman spectral signature associated with infection. The multivariate chemometric analysis technique, principal component analysis (PCA) was applied to decompose the spectral data into components and attempt to identify subtle changes to biological components within tissue sections which could differentiate infected tissue burden from non-infected samples.

Materials and methods

Infections and tissue preparation

Procedures on mice were approved following local ethical review by the University of Glasgow Animal Procedures and Ethics Committee and were performed in strict accordance with the UK Home Office Animals (Scientific Procedures) Act 1986 (Project Licence No. P2F28B003). Two female, BALB/c mice (Harlan, Bicester, UK; 6-8 weeks old) were infected with asynchronous *P. berghei* ANKA, and euthanised when peripheral blood parasitemia reached 5 %. At this level, although high, the infection is asymptomatic in BALB/c mice. Spleens were removed from these and from two uninfected control mice and embedded in tissue freezing medium (Tissue-Tek O.C.T.).25 This freezing medium was used to preserve the tissue structure. Frozen tissue blocks were then positioned in a cryostat chamber at -22°C, cut into sections with a thickness of 10 µm and placed on poly-L-lysine glass slides with Tissue-Tek O.C.T. Ten tissue sections were taken from the infected spleens, along with a further ten from the uninfected spleens. Tissue sections on glass slides were stored at -20°C prior to analysis. Spleen tissue was chosen as it is a key tissue for the sequestration of the parasite.

Reference spectra

Synthetic hemozoin was prepared using methods reported by Egan *et. al*.[26,27] (full synthetic method is given in ESI S1) and a 2.5 mg/mL solution prepared with PBS (10 mM, pH 7.2). Hemoglobin was purchased from Sigma-Aldrich and a 10 mg/mL solution prepared with PBS. 100 µL of each solution were spotted on glass coverslips and allowed to dry overnight before analysis.

Raman spectroscopy

Tissue sections were left to thaw at room temperature, washed once with PBS (10mM, pH 7.2) and finally rinsed in $d.H_2O$. Raman mapping was performed using a Renishaw inVia Raman spectrometer equipped with 532 nm laser excitation (5 % laser power, 1 mW) and an 1800 l/mm grating. Raman images of uninfected and infected malaria tissue were recorded using a x50 objective (NA = 0.75) with an integration time of 3 s per spectrum, a step size of 1 µm, and in the spectral range of 680 – 2330 cm^{-1}.

Hemoglobin and hemozoin reference spectra were collected using a x20 objective, 30 s acquisition time per spectra and a 532 nm laser excitation (1 % laser power, 0.1 mW).

Data pre-processing

In all datasets, a cosmic ray removal algorithm was first applied within WiRE 4.2 software. This algorithm sets values for width and height of features to detect potential cosmic rays, which are then accepted or rejected by the programmer. Noise filtering was then applied within the same software, to reduce the level of random noise within the data whilst maintaining the important Raman spectral features. This pre-processing method applies a form of PCA to the dataset, which subsequently provides scores and loadings for each principal component (PC) to determine whether components primarily relate to real Raman signals or noise. The optimum number of PCs, which describe all the real Raman signal with minimal noise interference, can then be selected for each Raman map. Raman spectra were baseline corrected using an asymmetric least square smoothing algorithm[28] operating in Matlab R2013a software (The MathWorks, Natick, MA, USA). Finally, all datasets were truncated so only the fingerprint region of interest was studied (700 – 1700 cm^{-1}).

The reference spectra shown are the average of five spectra, that were baselined using the same asymmetric least square smoothing algorithm as above.

Empirical analysis

In this study, the empirical analysis focused on the ratio of the Raman peak intensity at ~745 cm^{-1} (ν_{15} hemoglobin)[29,30], to the peak intensity at ~1307 cm^{-1} (ν_{21} hemoglobin & lipids)[18,29] for both tissue types. An unpaired student's t-test was used to assess whether the difference in the Raman intensity ratio (I_{745}/I_{1307}) between non-infected and infected tissues was statistically significant.[18,19] To manage the data for analysis, all infected Raman maps were combined to give one large data matrix containing thousands of Raman spectra, the same process was carried out with the uninfected data. These were then averaged to leave 43 final infected Raman spectra and 43 control spectra (n = 43). These data were subsequently used for empirical and multivariate analysis. The intensity ratios for all samples were plotted to observe sample distribution, along with the average intensity ratio plot for both the control and infected tissue. This analysis was performed on the same data set, used for the PCA model.

Multivariate analysis

PCA was applied to highlight any spectral separation between the control and infected data sets using Matlab software version R2013a (The MathWorks, Natick, MA, USA). Multiple maps for both tissue types were combined and averaged to give 43 final spectra for both the control and infected tissue data sets. The dataset was then normalised and mean centred prior to PCA being applied. Principal component one (PC1) was then plotted against principal component two (PC2). The loadings plots were also plotted to determine correlation. All analysis within Matlab software was performed using custom scripts.

Results and Discussion

Average spectra of non-infected and malaria parasite infected tissue

In this study two approaches were used to analyse the large spectral data sets. Firstly, spectral features were studied and changes in relative peak intensity investigated using intensity ratio maps and empirical analysis. The second approach used PCA to determine the primary spectral features resulting in correlations or anti-correlation between the infected and non-infected tissue, by creating principal components to explain the data set variance in an unsupervised manner.

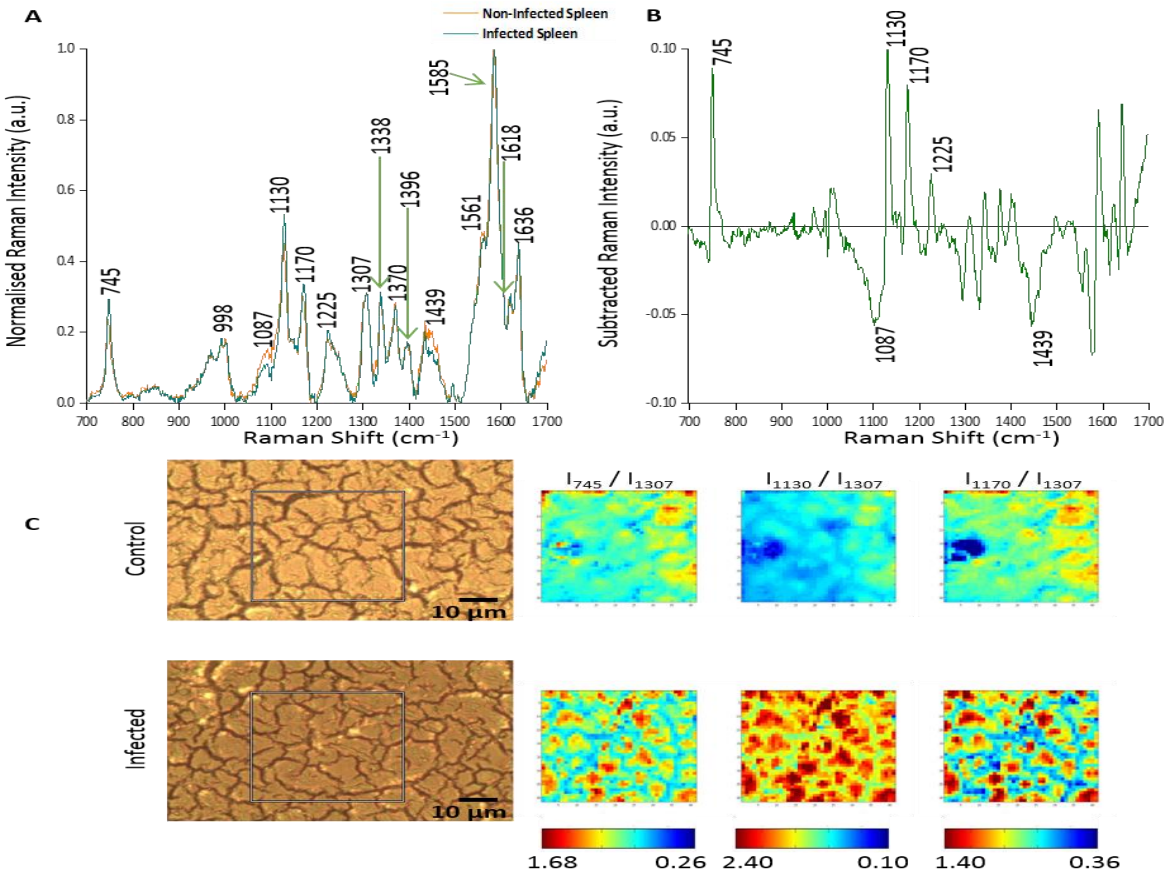

Figure 1: Analysis of Raman peak intensity for control and *P. berghei*-infected tissue sections. (A) Averaged, normalised spectra from a mapped area of control and infected tissue. Spectra were then normalised against the peak at 1585 cm^{-1}. Tentative peak assignments are also given in Table 1. (B) Subtracted Raman spectrum. The average, normalised control spectrum was subtracted from the average, normalised infected spectrum, both shown in (A), to highlight any potential biological components that were being altered within the malaria infected tissue. (C) Image shows white light images of both tissue sections, with the grey box indicating the area that was mapped, along with peak intensity ratio maps for selected Raman peaks. Intensity ratio maps were created using the peak intensities for: 745 cm^{-1}, 1130 cm^{-1}, 1170cm^{-1}, and 1307 cm^{-1} (I_{745} / I_{1307}; I_{1130} / I_{1307}; I_{1170} / I_{1307}). These ratio maps visually show relative changes in the intensity of these Raman peaks within the area of *P. berghei*-infected tissue that was mapped compared to the uninfected area. These maps suggest an increase or alteration to some key biological components within the infected tissue including, multiple hemoglobin vibrations[29], lipids[31], and proteins[30].

Figure 1A shows the averaged, normalised Raman spectra obtained from a non-infected (control) tissue map and a *P. berghei* infected mouse spleen tissue map. Both tissue types showed a very similar spectral profile, highlighting that the biochemical compositions were closely linked. Tentative peak assignments of the Raman bands are listed in Table 1. However, differences in the relative Raman peak intensities for infected *vs*. control tissue were observed. These were highlighted through subtraction of the average, normalised control spectra from the infected (Figure 1B). This emphasised some peaks that appeared to increase (~745, 1130, 1170 and 1225 cm^{-1}) and decrease (~1087 and 1439 cm^{-1}) in Raman signal intensity within the *P. berghei* infected tissue compared with the control. This change in relative peak intensity suggests an alteration in the biological composition of the spleen at this level of infection, characterised by changes in level and/or composition of the biological species assigned to these Raman signals.

Intensity ratio maps (Figure 1C) were created to visually show these relative peak changes, using the 1307 cm^{-1} peak as a constant background. These heat intensity maps showed a clear overall increase in the peak intensity ratios within the infected mapped areas compared to the control samples. This suggests alterations to biological components including hemoglobin[29,32] (~745, 1130 and 1170 cm^{-1}), lipids[30] (~1130 cm^{-1}) and other proteins[30] (~1170 cm^{-1}) at this level of *P. berghei* infection. Ratio maps were also created for different samples to show this overall increase was common throughout the infected tissue (ESI Figure S2). Within these maps, for both uninfected and infected samples, particularly intense regions are present (Figure 1C and ESI Figure S2). This can be explained through enhanced Raman intensity from resonance contributions of the biological components within these areas of tissue. These ratio maps visually show relative changes in biological peaks in a simple manner and can be used alongside empirical analysis and PCA to aid in classification of tissue types from Raman spectroscopy data.

Table 1. Tentative peak assignments for the main peaks observed in the spectral profile for both non-infected and *P. berghei* infected spleen samples.

Raman Shift (cm^{-1})	Assignment[a]
745	ν_{15} Hb [ν(pyr breathing)]
998	Proteins (Phe), ν_{45} Hb [$\nu(CC)_{asym}$]
1087	DNA / Nucleic acids [ν_s (PO_2^-), ν (CC)], Hb
1130	Lipids, ν_5 Hb [$\delta(=CH_2)_4$]
1170	Proteins (Tyr), ν_{30} Hb [ν(pyr half -ring)$_{asym}$]
1225	Proteins (Amide III), ν_{13}/ν_{42} Hb [δ(CH)]
1307	Lipids, ν_{21} Hb [δ(CH)]
1338	Nucleic acid modes, ν_{41} Hb [ν(pyr half-ring)$_{sym}$]
1370	ν_4 Hb [ν(pyr half-ring)$_{sym}$]
1396	CH_2 deformation, ν_{20} Hb [ν(pyr quarter-ring)]
1439	Lipids [$\delta(CH_2)$]
1561	ν_{11} Hb [ν(CC)]
1585	ν_{37} Hb [$\nu(CC)_{asym}$]
1618	ν_{19} Hb [$\nu(CC)_{asym}$]
1636	Proteins (Amide I), ν_{10} Hb [$\nu(CC)_{asym}$]

a Abbreviations: ν – stretch vibration; δ – in-plane bending vibration; sym – symmetric; asym – asymmetric; Hb – hemoglobin; Phe – phenylalanine; Tyr – tyrosine. Assignments from ref. [16, 18,29-31]

Empirical analysis of Raman spectra

Diagnostic algorithms based on peak intensity ratios have been widely employed in the literature for tissue classification using Raman spectroscopy.[18,19,23] These have been shown to successfully correlate variations in tissue spectra with tissue pathology[19] in a simple manner.

An empirical analysis based on the peak intensity ratio of two Raman bands was used for tissue classification within this study. Figure 2A shows the scatter plot of the ratio of Raman peak intensity at 745 cm^{-1} to 1307 cm^{-1} (I_{745}/I_{1307}) for the 43 averaged *P. berghei* infected samples and 43 uninfected samples. A clear separation was observed in the scatter plot for the two data sets, with replicate data within each tissue type being grouped closely together, indicating little intra-sample variation in the intensity ratios. The mean ratio values (mean ± std. dev.) for both control (0.903 ± 0.015) and infected (1.119 ± 0.021) data sets were also plotted (Figure 2B). It was shown that the differences between the mean ratios for each tissue type were statistically relevant (unpaired student's t-test, $p < 0.0001$). Infected tissue showed a higher ratio value compared with control, this could be explained by the increase in heme-based Raman vibrations (~745 cm^{-1} assigned to ν_{15} Hb[29]) due to the presence of hemozoin within the infected samples.

From these results, this intensity ratio is a potential simple and reliable marker to indicate the presence of infection. It has also been shown that other peak ratios can also be used to classify the two tissue types with good results (ESI Figure S3). However, this method does not consider the entire Raman spectrum. To help improve tissue analysis and classification, PCA was employed to highlight the most diagnostically significant Raman peaks.

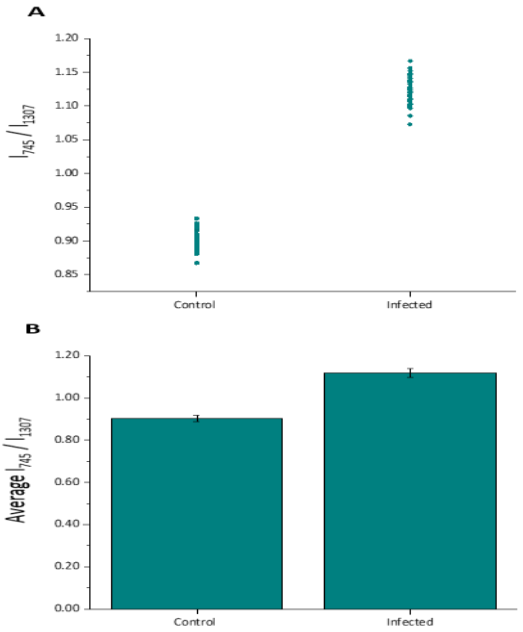

Figure 2: Empirical analysis results. (A) Scatter plot of peak intensity ratios (I_{745}/I_{1307}) for 43 average Raman spectra from all the control and malaria infected mice spleen tissue that were mapped. A clear separation of the two data sets was observed, with little intra-sample variability. (B) Average intensity ratio plots for the control (0.903 ± 0.015) and infected (1.119 ± 0.021) data sets. This difference in mean ratios was shown to be statistically relevant (unpaired Student's t-test, $p < 0.0001$).

Principal component analysis

PCA was used to analyse this data set to better distinguish the spectral differences between the non-infected and infected spleen tissue. Figure 3 shows the scores plot for PC1 (97.6 % variance) and PC2 (1.45 % variance), along with the corresponding loadings vectors. As can be seen from the scores plot (Figure 3A) PC1 was primarily responsible for the separation of the two tissue types. The loadings plot (Figure 3B) for PC1 indicated that the peaks in the negative half of the plot were spectrally important for describing the separation of the infected tissue (~750, 1130, 1170, 1225, 1370, 1529, 1588 and 1628 cm^{-1}), with the latter few being more indicative of hemozoin than hemoglobin. The negative peaks at ~1529, 1588 and 1628 cm^{-1} matched closely with that of the hemozoin reference spectra in Figure 4 (core structures of hemoglobin and hemozoin shown in ESI S4 to highlight structural similarities) and therefore suggested detection of the insoluble pigment by Raman. The negative ~1370 cm^{-1} peak was present in both reference spectra; however, it was much more prominent within hemozoin and so suggested that hemozoin was contributing to this peaks appearance within the PC1 loadings plot. It is well known that hemozoin accumulates within the spleen[8,9] (presence of hemozoin within the infected spleen can be seen in stained tissue images, ESI S5), therefore it follows that there will be an associated increase in concentration of heme-based Raman vibrations. This is clearly shown in this PCA model as many of these peaks separating the infected tissue from the uninfected samples can be assigned to heme-vibrations, including hemozoin. Although other proteins and lipids will be present and exhibit Raman bands in similar positions to those of hemoglobin (~1130, 1170, 1225 & 1396 cm^{-1}), resonance effects would mean hemoglobin will tend to dominate the spectra (excitation in the regions of Q-absorption bands)[29,32,33], with the other proteins and lipids having only small contributions to the observed spectra.

Within the positive peaks in the PC1 loadings plot, the relatively broad ~1087 cm^{-1} peak is likely to have a significant contribution from hemoglobin (Figure 4), however, its broadness suggested contributions from other components. Raman bands within this region can also be assigned to C-C and O-P-O vibrations of nucleic acids.[18,30] The other prominent positive peak at ~1439 cm^{-1} can mainly be assigned to Raman vibrations from lipids[18,31], although it may also have slight hemoglobin contributions (~1432 cm^{-1} peak in reference spectra). Analysis of the PC1 loadings plot indicated that at this level of *P. berghei* malaria infection Raman spectroscopy can clearly detect hemozoin accumulation within the spleen, with the positive peaks (~1087

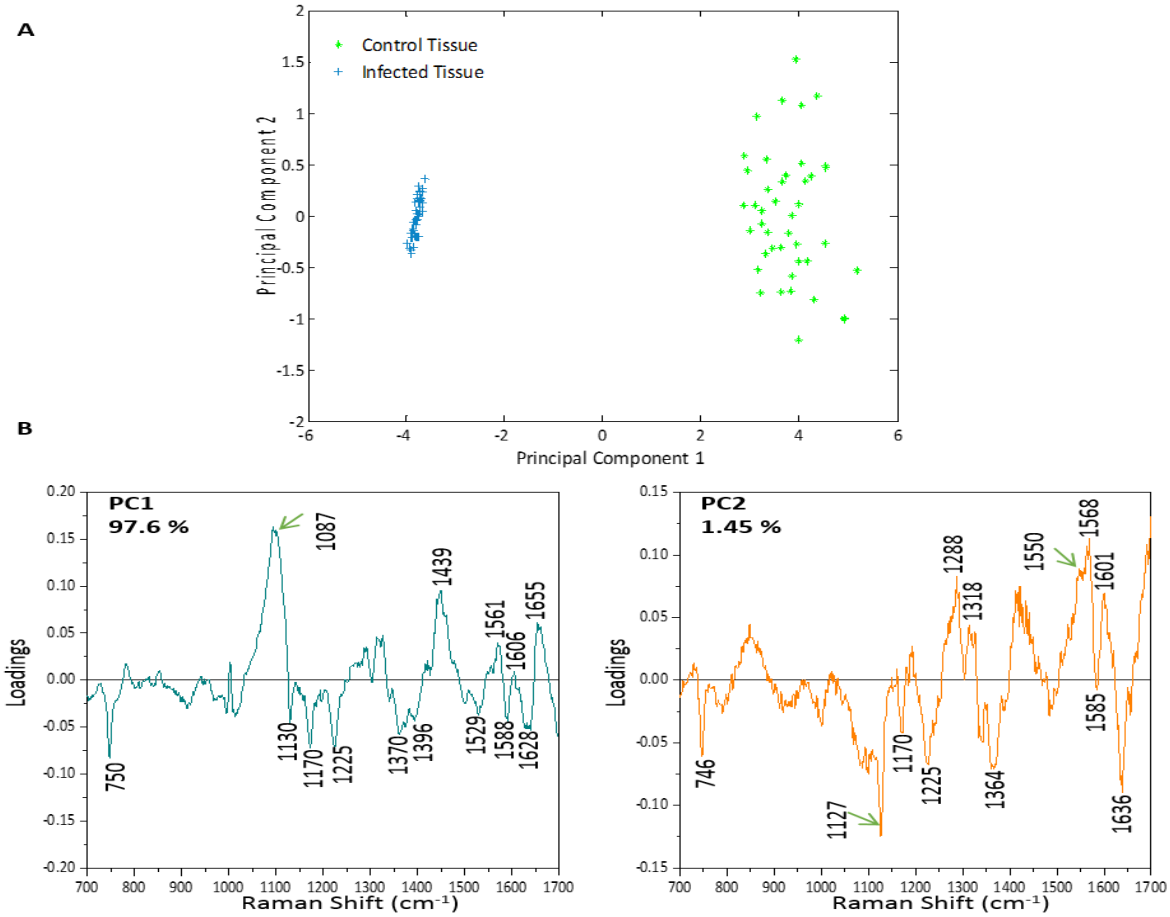

Figure 3. PCA plot for control and malaria infected samples from mouse spleen tissue sections. (A) Scores plot showing very clear separation of the control (green) and infected (blue) data sets. Separation is occurring mainly along PC1, with little separation along PC2. (B) Loadings plots for PC1 and PC2, with the main peaks in both indicated. The peaks in the negative half of PC1 are responsible for the separation of the infected samples along PC1 away from the control samples.

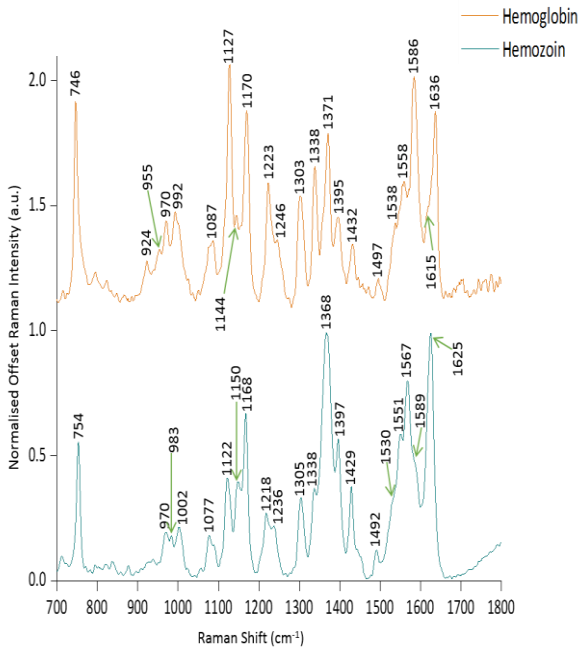

Figure 4: Raman reference spectra of hemoglobin and hemozoin. The spectra shown are the average of five spectra and have been baseline corrected, normalised to the highest peak and offset for clarity. Key Raman bands are also indicated.

and 1439 cm^{-1}) indicating that as the amount of hemozoin increases within the spleen there is a corresponding change to hemoglobin and some lipids/nucleic acid vibrations.

PC2 describes little separation between the control and infected samples. From the PC2 loadings plot (Figure 3B) the positive peaks (~1550, 1568, 1601 cm^{-1}) originate mainly from hemoglobin vibrations, whereas the negative peaks have contributions from hemoglobin as well as from other proteins[18,30] (~1170, 1225 and 1636 cm^{-1}) and lipids[31] (~1127 cm^{-1}). This PCA analysis indicates that Raman imaging can easily distinguish between *P. berghei* infected spleen tissue from uninfected samples, through identification of hemozoin accumulation and alterations to other key biological components.

Conclusions

In conclusion, a combination of Raman imaging with multivariate analysis resulted in very clear discrimination of *P. berghei* infected tissue from non-infected samples. Separation highlighted an overall increase in heme-based Raman vibrations within the infected samples, which correlates with the accumulation of hemozoin within the spleen contributing to this. Hemozoin detection was clear with the identification of key peaks occurring ~1370, 1529, 1588, and 1628 cm^{-1} which matched closely with the reference spectra. Chemometric analysis also showed that at the level of *P. berghei* infection reported here, changes to hemoglobin and some other lipid/nucleic acid vibrations corresponded with an increase in hemozoin content within the spleen. Other proteins (tyrosine ~1130 cm^{-1}, and Amide III ~1225 cm^{-1}) and lipids (~1130 cm^{-1}) were also contributing to the separation of infected tissue from control. However, due to the resonance effects of heme-based compounds the separation contribution from these biological components would have been small.

The use of peak ratio maps and empirical analysis also highlighted changes to the biological components as you move towards an infected tissue state. These two simple data analysis methods could be used as tools in combination with the PCA to help improve efficiency of Raman tissue analysis and classification.

As the Raman imaging technique used in this study had a short penetration depth, it would not be suitable for *in vivo* diagnostics. However, with the development of spatially offset Raman spectroscopy, which allows accurate analysis through millimetres of material when obscuring barriers such as skin are present[34,35], this may allow for biochemical information from tissue to be detected *in vivo* in the near future. Overall, this approach demonstrates the potential use of Raman spectroscopy to provide detailed chemical information from both malaria parasite infected and control tissue and when coupled with PCA, discrimination due to infection burden is achievable between the two sample groups.

Conflicts of interest

There are no conflicts to declare.

Acknowledgements

This work was supported by the University of Strathclyde. Data associated with research published in this paper is accessible at: http://dx.doi.org/10.15129/89483183-40b2-4ebb-8b10-43a4615e40db and http://dx.doi.org/10.15129/b069f380-61ae-494d-9419-dcdf28a5b160.

Notes and references

1 World Health Organisation. *World Malaria Report 2015*, 2015.
2 Aird, W. C.; Mosnier, L. O.; Fairhurst, R. M., *Blood*, 2014, **123**, 163–168.
3 CDC:MalariaParasites,https://www.cdc.gov/malaria/about/biology/parasites.html (accessed Sep 22, 2017).
4 Frosch, T.; Koncarevic, S.; Becker, K.; Popp, J., *Analyst*, 2009, **134**, 1126–1132.
5 Coronado, L. M.; Nadovich, C. T.; Spadafora, C., *Biochim. Biophys. Acta*, 2014, **1840**, 2032–2041.
6 Frosch, T.; Koncarevic, S.; Zedler, L.; Schmitt, M.; Schenzel, K.; Becker, K.; Popp, J., *J. Phys. Chem. B*, 2007, **111**, 11047–11056.
7 Boura, M.; Frita, R.; Góis, A.; Carvalho, T.; Hänscheid, T., *Trends Parasitol*., 2013, **29**, 469–476.
8 Ferrer, M.; Martin-Jaular, L.; De Niz, M.; Khan, S. M.; Janse, C. J.; Calvo, M.; Heussler, V.; Del Portillo, H. A., *Parasitol. Int*., 2014, **63**, 195–205.
9 Del Portillo, H. A.; Ferrer, M.; Brugat, T.; Martin-Jaular, L.; Langhorne, J.; Lacerda, M. V. G., *Cell. Microbiol*., 2012, **14**, 343–355.
10 Engwerda, C. R.; Beattie, L.; Amante, F. H., *Trends Parasitol*., 2005, **21**, 75–80.
11 Franke-Fayard, B.; Fonager, J.; Braks, A.; Khan, S. M.; Janse, C. J., *PLoS Pathog*., 2010, **6**, 1-10.

12 Autino, B.; Corbett, Y.; Castelli, F.; Taramelli, D. Mediterr. J., *Hematol. Infect. Dis*., 2012, **4**, 1-12.
13 Khoury, D. S.; Cromer, D.; Best, S. E.; James, K. R.; Kim, P. S.; Engwerda, C. R.; Haque, A.; Davenport, M. P., *Infect. Immun*., 2014, **82**, 212–220.
14 Wood, B. R.; Langford, S. J.; Cooke, B. M.; Glenister, F. K.; Lim, J.; McNaughton, D., *FEBS Lett*., 2003, **554**, 247–252.
15 Wood, B. R.; Hermelink, A.; Lasch, P.; Bambery, K. R.; Webster, G. T.; Khiavi, M. A.; Cooke, B. M.; Deed, S.; Naumann, D.; McNaughton, D., *Analyst*, 2009, **134**, 1119–1125.
16 Hobro, A. J.; Konishi, A.; Coban, C.; Smith, N. I., *Analyst*, 2013, **138**, 3927–3933.
17 Hackett, M. J.; Aitken, J. B.; El-Assaad, F.; McQuillan, J. a; Carter, E. a; Ball, H. J.; Tobin, M. J.; Paterson, D.; de Jonge, M. D.; Siegele, R.; Cohen, D. D.; Vogt, S.; Grau, G. E.; Hunt, N. H.; Lay, P. A., *Sci. Adv*., 2015, **1**, 1–13.
18 Kochan, K.; Marzec, K. M.; Chruszcz-Lipska, K.; Jasztal, A.; Maslak, E.; Musiolik, H.; Chłopicki, S.; Baranska, M., *Analyst*, 2013, **138**, 3885–3890.
19 Teh, S. K.; Zheng, W.; Ho, K. Y.; Teh, M.; Yeoh, K. G.; Huang, Z., *Br. J. Cancer*, 2008, **98**, 457–465.
20 Frank, C. J.; McCreery, R. L.; Redd, D. C., *Anal. Chem*., 1995, **67**, 777–783.
21 Huser, T.; Chan, J., *Adv. Drug Deliv. Rev*., 2015, **89**, 57–70.
22 Hobro, A. J.; Pavillon, N.; Fujita, K.; Ozkan, M.; Coban, C.; Smith, N. I., *Analyst*, 2015, **140**, 2350–2359.
23 Huang, Z.; McWilliams, A.; Lui, H.; McLean, D. I.; Lam, S.; Zeng, H., *Int. J. Cancer*, 2003, **107**, 1047–1052.
24 Haka, A. S.; Shafer-Peltier, K. E.; Fitzmaurice, M.; Crowe, J.; Dasari, R. R.; Feld, M. S., *Proc. Natl. Acad. Sci. U. S. A*., 2005, **102**, 12371–12376.
25 Tissue-Tek O.C.T Compound and Cryomolds http://www.sakura.eu/Our-products/item/11/Cryotomy/48/Tissue-Tek-OCT-Compound-and-Cryomolds (accessed Sep 15, 2017).
26 Egan, T. J.; Rossa, D. C.; Adamsb, P. A., *FEBS Lett*., 1994, **352**, 54–57.
27 Egan, T. J.; Mavuso, W. W.; Ncokazi, K. K., *Biochemistry*, 2001, **40**, 204–213.
28 Eilers, P. H. C.; Boelens, H. F. M., *Life Sci*., 2005, 1–26.
29 Rusciano, G.; De Luca, A. C.; Pesce, G.; Sasso, A., *Sensors*, 2008, **8**, 7818–7832.
30 Movasaghi, Z.; Rehman, S.; Rehman, I. U., *Appl. Spectrosc. Rev*., 2007, **42**, 493–541.
31 Krafft, C.; Codrich, D.; Pelizzo, G.; Sergo, V., *Analyst*, 2008, **133**, 361–371.
32 Polakovs, M.; Mironova-Ulmane, N.; Kurjane, N.; Reinholds, E.; Grube, M., *Proc. SPIE*, 2008, **7142**, 1-8.
33 Spiro, T. G.; Strekas, T. C., *J. Am. Chem. Soc*., 1974, **96**, 338–345.
34 Stone, N.; Matousek, P., *Cancer Res*., 2008, **68**, 4424–4430.
35 Keller, M. D.; Majumder, S. K.; Mahadevan-Jansen, A., *Opt. Lett*., 2009, **34**, 926–928.